Microstructure development during pyrolysis of wet-laid nonwoven-based CFRP for the manufacturing of Ceramic Matrix Composites (CMC)

Fiona Kessel , Luis Baier , Nils Hensch , Martin Frieß , Anna Markic , Thomas Bratzdrum , Dietmar Koch

PII: S2666-5395(25)00102-6
DOI: https://doi.org/10.1016/j.oceram.2025.100835
Reference: OCERAM 100835

To appear in: *Open Ceramics*

Received date: 1 July 2025
Revised date: 8 August 2025
Accepted date: 16 August 2025

Please cite this article as: Fiona Kessel , Luis Baier , Nils Hensch , Martin Frieß , Anna Markic , Thomas Bratzdrum , Dietmar Koch , Microstructure development during pyrolysis of wet-laid nonwoven-based CFRP for the manufacturing of Ceramic Matrix Composites (CMC), *Open Ceramics* (2025), doi: https://doi.org/10.1016/j.oceram.2025.100835

Microstructure development during pyrolysis of wet-laid nonwoven-based CFRP for the manufacturing of Ceramic Matrix Composites (CMC)

Authors

Fiona Kessel*[1]	https://orcid.org/0000-0001-9417-7162
Luis Baier[1]	https://orcid.org/0009-0008-6537-5870
Nils Hensch[1]	https://orcid.org/0009-0002-4680-5130
Martin Frieß[1]	https://orcid.org/0000-0002-4425-8244
Anna Markic[2]	
Thomas Bratzdrum[3]	
Dietmar Koch[3]	https://orcid.org/0000-0003-4504-8721

[1] German Aerospace Center
[2] Reutlingen University
[1] Augsburg University
* corresponding author

Keywords

a) Ceramic matrix composites (CMC)
b) Wet-laid nonwoven
c) Pyrolysis
d) Phenolic resin

Abstract

Fiber reinforcement plays a critical role in defining the properties of ceramic matrix composites (CMCs). Among various textile technologies, wet-laid nonwovens have gained attention because previous studies have shown that their method of production significantly influences ceramic formation during liquid silicon infiltration (LSI) [1]. This study investigates *in-situ* microstructural evolution during pyrolysis using microscopy in a small-scale furnace. Two carbon fiber-reinforced polymer (CFRP) types were examined: *single filament* and *fiber bundle* wet-laid nonwovens. Thermal analysis revealed distinct behaviors. In *single filament* samples, key cracking occurred around 610 °C due to matrix weakening and stress release. In contrast, *fiber bundle* samples showed crack formation at 150–300 °C and above 700 °C, driven by outgassing, partial matrix detachment, and matrix shrinkage. These mechanisms result in SiC-rich structures for *single filament* reinforced materials and carbon-rich, short fiber composites for bundle reinforced materials. The findings support tailored reinforcement design for application-specific CMC properties.

Graphical abstract

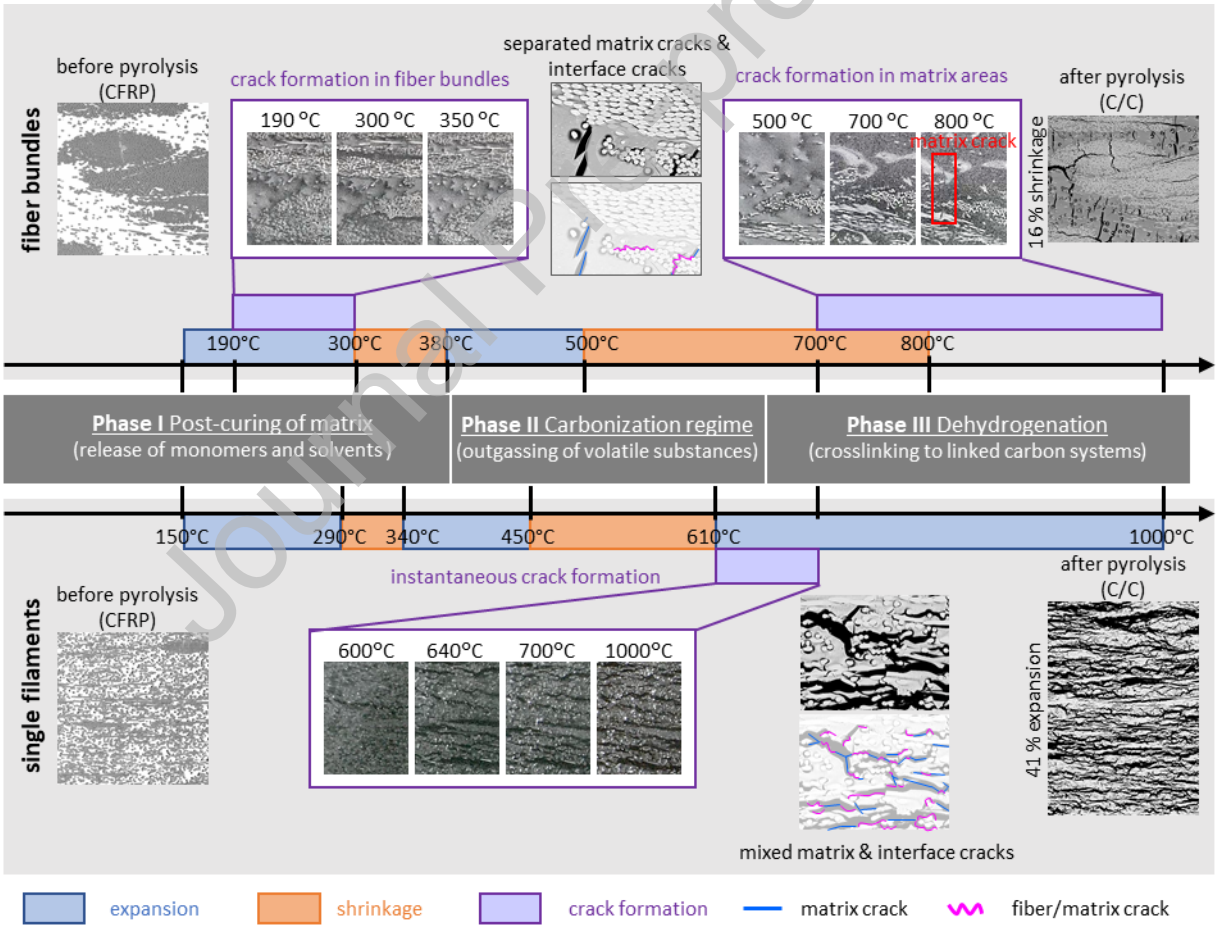

Figure 1 – Scheme of the processes during the pyrolysis of different wet-laid nonwoven based CFRP materials.

1 Introduction

Ceramic matrix composites (CMC) have been studied since the 1980s and have their application origins in aerospace, where they were used as a damage-tolerant variant of otherwise brittle ceramics for heat protection (TPS) during re-entry [2-4]. Since then, their production and application areas have been greatly expanded and a variety of different CMC materials are commercially available or being researched. One of the most economical processes for the production of C/C-SiC (carbon fiber reinforced carbon and silicon carbide) is liquid silicon infiltration (LSI). In this process, a CFRP (carbon fibers reinforced polymer) is produced, which is subsequently pyrolyzed and then infiltrated (siliconized) with liquid silicon [4]. The resulting C/C-SiC is characterized by high thermal resistance, constant properties over a wide temperature range and high fracture toughness. The key technology for achieving these properties is a suitable embedding of the fibers in the matrix, which must be accompanied by a weak fiber/matrix interface [5, 6]. This ensures that cracks that occur in the brittle matrix are deflected along the interface when the material is stressed or damaged. This leads to energy dissipation when damage occurs and prevents the brittle failure that is otherwise common for ceramics. The microstructure of the material is crucial to achieving this behavior. It is important that a macroscopic crack network is created during the production of the material during pyrolysis. This ensures that the majority of the fibers are embedded in the carbon matrix as a solid block and are therefore barely accessible to molten silicon during siliconization. This ensures that silicon and carbon only react to form the ceramic silicon carbide matrix in the large crack areas. The bond between the matrix (SiC) and carbon (fibers and C-matrix) is strong due to morphological interlocking, but weak in the carbon blocks (fibers and C-matrix), thus the high fracture toughness of weak fiber matrix interface materials can be achieved [6].

Wet-laid nonwovens are one interesting fiber reinforcement option for short-fiber C/C-SiC ceramics. They have only a small proportion of fibers in through thickness orientation (z-direction, almost zero percent) which allows, compared to needled nonwovens, good compression of the textile and thus a high fiber volume fraction in the CFRP. Their use is currently being investigated in the field of brake disc technology and missile tips [1, 7]. Previous work has shown that variations in the wet-laid nonwoven production and resulting different nonwoven styles have a significant influence on the resulting material microstructure and properties [1]. Nonwovens with a high proportion of individual filaments exhibit a strong micro-crack pattern after pyrolysis and have a high silicon carbide content after siliconization (67.8 %) (Figure 2 left). In contrast, nonwovens, in which the filaments are present in a largely compact short fiber bundle structure, exhibit a more block-like crack pattern. This is similar to that of conventional short fiber-reinforced C/C-SiC and results in a typical microstructure (Figure 2 right) [1]. Few publications focus on the influence of morphology of the fiber reinforcement on the formation of different crack structures during pyrolysis, under otherwise identical manufacturing conditions.

According to Jenkins et al. phenolic resins which are thermosets are pyrolyzed in four stages depending on the temperature: consolidation (< 350 °C), the carbonization regime (300 °C - 500 °C), dehydrogenation (500 °C - 1200 °C) and annealing (> 1200 °C) [8]. In the first phase, the resin is cross-linked (cured) and monomers and solvents are split off through outgassing. During the second phase - the main pyrolysis - oxygen, nitrogen compositions and chlorides are split off. This results in a significant mass loss and larger carbon chains. In the third phase remaining hydrogen decomposes

and the carbon chains cross-link parallel to each other. In the final phase, the crystallinity of the carbon network increases and defects are diminished.

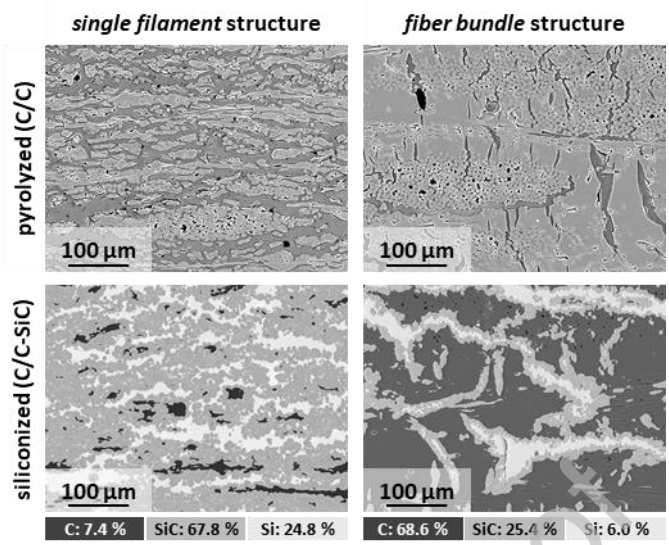

Figure 2 – Microstructure of different wet-laid nonwoven based CMC after pyrolysis and after siliconization [1]

Trick et al. investigated the pyrolysis of phenolic resin based CFRP using FTIR analysis in order to quantitatively determine the released gas species [9]. They identified three main phases of pyrolysis for the formation of C/C composites: 1. intermolecular crosslinking (300-550 °C), 2. breaking of crosslinks (400 - 800 °C), and 3. formation of benzene rings with hydrogen splitting (560 - 900 °C). This agrees well with the results found by Torres-Herrador et al. [10]. Schulte-Fischedick et al. investigated the formation of cracks in fabric-reinforced CFRP during the pyrolysis process using *in-situ* thermal microscopy [11, 12]. They explained how different crack formations can occur and defined the following mechanisms that lead to the formation of cracks during pyrolysis: 1. formation of pyrolysis gases, which diffuse into nano- and micropores and lead to a connected pore network due to increasing internal pressure, 2. volume shrinkage of the matrix due to carbon formation and resulting fiber/matrix debonding from approx. 490 °C, which leads to segmentation cracks perpendicular to fabric layers, 3. Crack propagation and deflection from approx. 550 °C leading to partial delamination parallel to fabric layers. The regular transverse cracks are primarily caused by macroscopic stresses due to matrix shrinkage and induce further fiber/matrix debonding; from 570 °C. The fiber orientation and the resulting internal stresses form the characteristic crack pattern in C/C-SiC. Jain et al. proposed a crack formation model considering fabric-reinforced C/C-SiC and the properties of fibers and matrix [13]. They generated microstructure images with typical crack patterns by variation of interfacial stresses between fibers and matrix and thermomechanical stresses due to expansion mismatch between fibers and matrix during pyrolysis. The resulting virtual microstructures were then validated by comparison with real microstructural images.

These investigations showed the principle influence of matrix, fiber reinforcement and pyrolysis on the formation of cracks in fabric reinforced C/C-SiC composites. However, there is still a lack in understanding how microstructure and cracks form in wet-laid nonwoven C/C-SiC materials. To clarify this, in this work *in-situ* pyrolysis thermal microscopy experiments are performed too evaluate

the influence of pyrolysis on the resulting material microstructure and to adjust the microstructure and resulting component properties, accordingly.

2 Experimental methods

2.1 Sample manufacturing

Two types of wet-laid nonwovens were selected for the investigation of crack formation defects, which, according to the findings of previous work, lead to different ceramics [1]. The fiber material was HTS 45, 12K, carbon fibers from Teijin Carbon Europe GmbH. The nonwovens were produced on a laboratory wet-laid nonwoven line at Reutlingen University with different process settings. Fibers with a cut length of 10 mm and a strong dispersion (dispersion at 2000 rpm for 10 minutes) of the fibers were selected for the *single filament* wet-laid nonwoven. The second *fiber bundle* nonwoven was produced with fiber25 mm long fibers and a low degree of dispersion (250 rpm for less than 3 minutes). Carbon fiber reinforced polymers (CFRP) were then produced according to the first step of the LSI process. For each wet-laid nonwoven type, a stack of layers was built with fibers for a target fiber volume fraction in the CFRP of 30 %. For molding, the layers were infiltrated with a phenolic resin and cured in a laminating press (Maschinenfabrik Lauffer GmbH & Co. KG) (190 ◦C for 2 h, at 0.65 bar). Bars 2 mm thick were then removed from the center panel area and polished at the cutting edge (polishing substrate diamond particles < 1 µm). Finally, round samples of suitable dimensions (diameter 4 mm, height 2 mm) for *in-situ* pyrolysis under the microscope were taken from the cross sections using a core drill (Figure 3left).

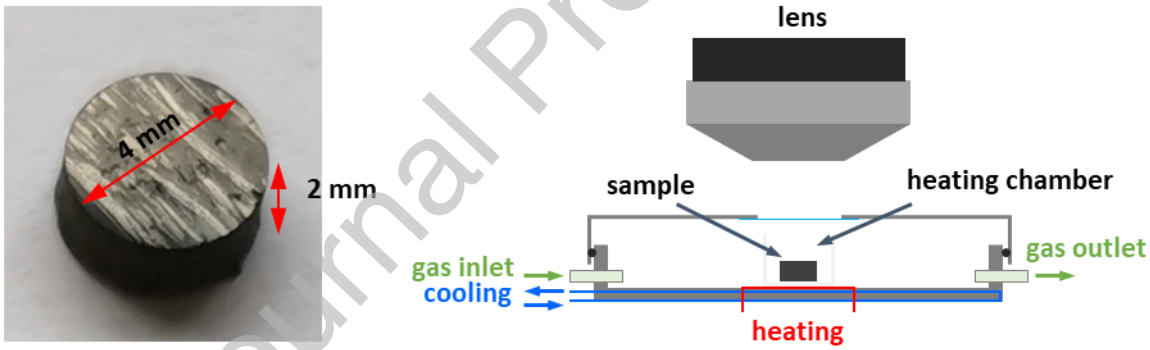

Figure 3 – left: CFRP sample for pyrolysis; right: Experimental setup for *in-situ* pyrolysis

2.2 Experimental setup

A Keyence digital microscope equipped with a VH-ZST objective and a connected camera was used to carry out the pyrolysis with simultaneous recording. This was extended with an *in-situ* furnace (TS1500) from Linkam scientific instruments. The heating chamber was pressurized with argon atmosphere and a continuous gas flow was applied during the process in order to pyrolyze in the absence of oxygen and to remove the resulting pyrolysis gases (Figure 3). The temperature profile of the process consists of three phases: Phase 1, room temperature → 300 °C, 100 K/min; Phase 2, 300 °C → 800 °C, 50 K/min; Phase 3, 800°C → 1000 °C, 100 K/min; cooling was uncontrolled. As most of the matrix conversion takes place in phase 2, the heating rate was reduced to allow the pyrolysis gases to evolve completely. During the whole process, a video of the sample area was recorded to interpret the specimen changes with temperature. Due to a shift in contrast and sample movement at higher temperatures the image quality deteriorated over the duration of the pyrolysis.

2.3 Analytical methods

Thermogravimetry (TG) measurements (STA 409, Netzsch-Gerätebau GmbH) were carried out with a heating rate of 10 K/min under nitrogen atmosphere to determine relevant temperatures during the conversion of the polymer matrix to the carbon matrix during pyrolysis. From this, TG information was used to identify relevant temperature ranges for the matrix during pyrolysis. The grammage (DIN EN ISO 9073-1) and the nonwoven thickness (DIN EN ISO 9073-2) were determined in accordance with the respective standards.

The thermal microscopy images were analyzed using two methods. In the first step, observed changes on the cross section of the sample surface were recorded and described in tabular form connected to the respective temperatures. The videos were afterwards analyzed using the Tracker software (version 6.2.0, Open Source Physics) to determine at which temperatures shrinkage or expansion effects quantitatively occur in the X, Y, and Z directions. The occurrence of cracks was analyzed by evaluation of individual images taken at relevant temperatures.

Additionally, the samples were analyzed both before and after pyrolysis using scanning electron microscopy (SEM, Gemini ultra plus from Zeiss Group). The SEM images were taken with an AsB detector (Angle selective Backscattered electron) and regions of interest (ROI) were determined in the CFRP state with an area of 1 mm x 1 mm. To correlate crack initiation and filament packing density, the ratio of area with filaments to total sample area was determined and sorted into three categories: low filament packing density, medium filament packing density, high filament packing density. For this categorization representative sections (0.2 mm x 0.2 mm, n=3 per category) were evaluated (Figure 4, left-hand side). The mean filament coverage was calculated for each category, and the category boundaries were defined as the midpoints between the mean values of adjacent categories, i.e., using half the difference ($\Delta/2$) between the corresponding average values. To categorize the areas in the ROI, a square grid of 20 x 20 units was defined with each square being assigned to one of the three categories. This results in a distribution of the category classes for the entire ROI area (Figure 4). After pyrolysis, the same grid was reapplied over the ROI, and the crack area fraction per ROI was quantified using a greyscale image analysis. This method was used to correlate the filament packing densities with the crack areas and to draw conclusions as to whether there was a direct influence. To determine the phase composition of the samples after siliconization, the images were analyzed using the ImageJ analysis software (version ImageJ 1.52p, Java 1.8.0_172 (64-bit)).

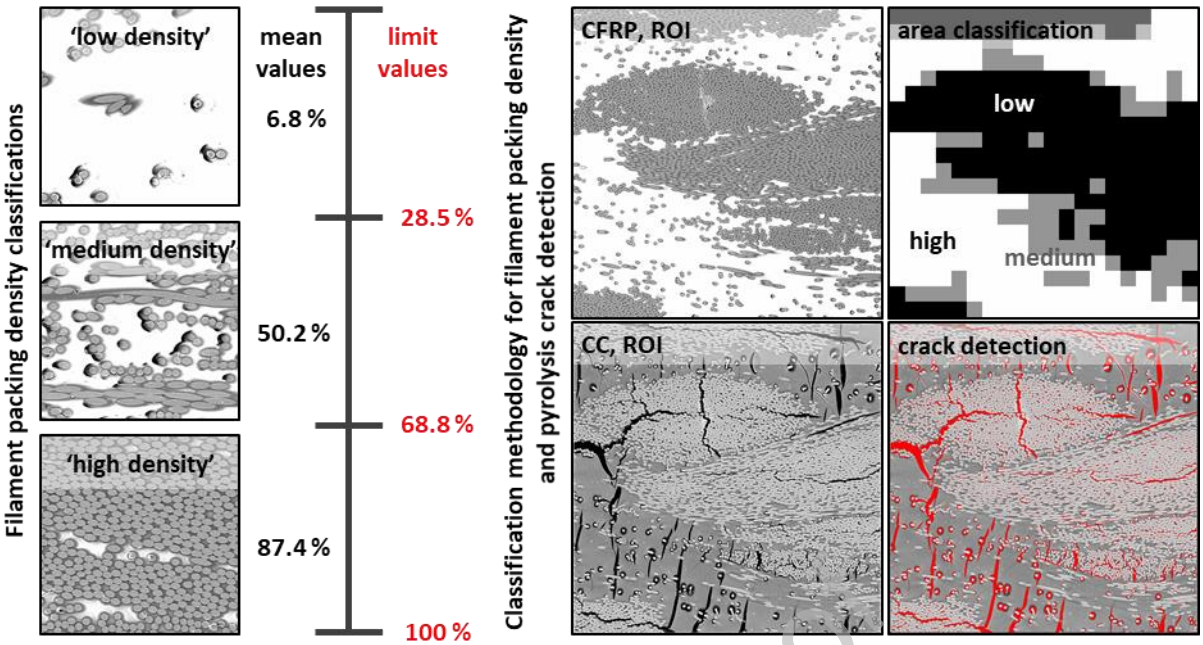

Figure 4 – Representative images used to classify boundaries between the fiber packing density categories; workflow for image segmentation into different fiber packing densities and the subsequent correlation of cracks after pyrolysis with the respective packing densities.

3 Results and discussion

3.1 Pre-analysis of resin and fiber preform

Prior to the *in-situ* pyrolysis, thermogravimetric (TG) measurements of the matrix were conducted to determine the onset and completion of the pyrolysis phases for the resin used. The TG results indicate that up to approximately 395 °C, a minor mass loss (9 %) occurs, marking the end of the first phase (Figure 5). This is followed by a second phase, when mass decreases significantly (an additional 35%, up to approximately 640 °C). Beyond this temperature, in third phase, mass loss is about 4 % up to 800 °C. The onset and endpoint of the phase with the highest mass loss are determined to be around 395 °C and 640 °C, but remains significant at the beginning of phase three due to the continued elimination of reaction products. In phase three further mass loss is minimized, and reorganization of carbon chains and bonds takes place. Compared to the phases described by Jenkins et al. [8], the onset and completion temperatures are slightly shifted to higher values. This suggests that a similar phase shift to higher temperatures can be expected for the composite material. However, the presence of all three pyrolysis phases within the investigated temperature range is confirmed.

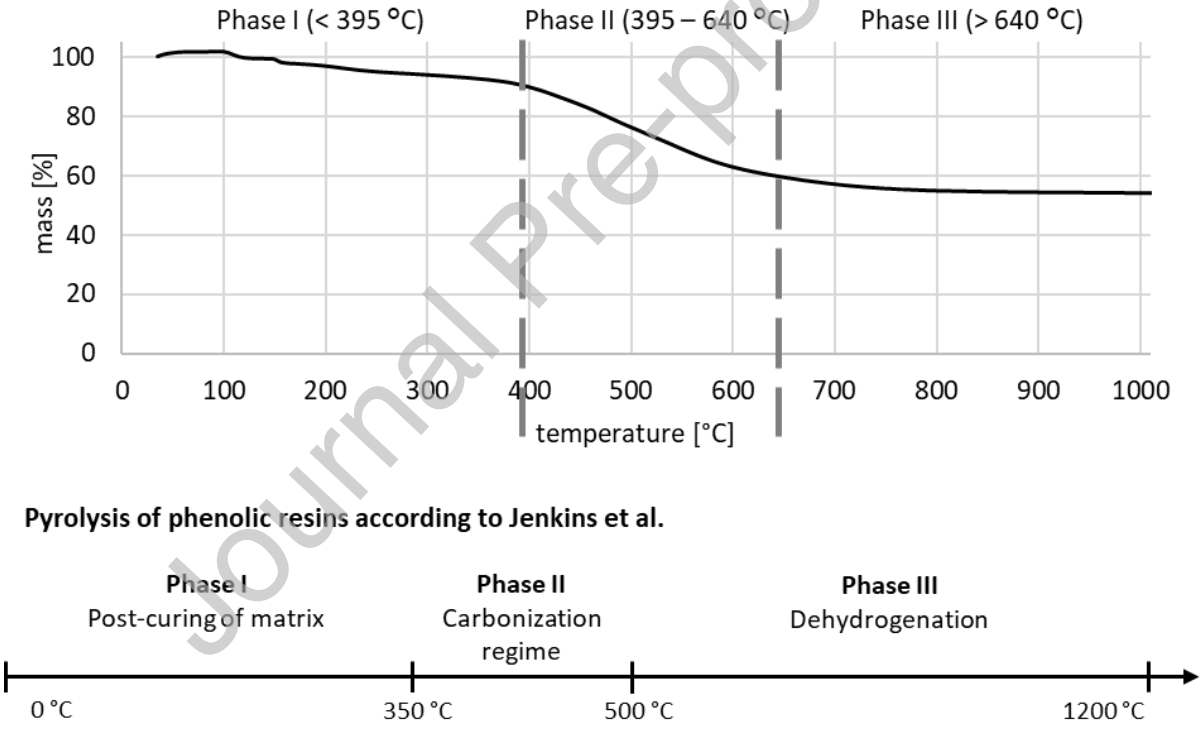

Figure 5 – above: results of mass loss over temperature via TG analysis; below: transformation phases of phenolic resins during pyrolysis according to Jenkins et al. [8]

Just like the matrix system, the nonwoven preforms were also analyzed prior to composite manufacturing. Both their area-specific mass and nonwoven thickness were determined (Figure 6). The results indicate that if the filaments are highly separated, the thickness of the nonwoven fabric is larger compared to the case if fiber bundles are used (Figure 6, left side). The measured area-specific mass further emphasizes this effect. As shown, the nonwovens composed of fiber bundles exhibit an even higher fiber content than those made of single filaments (Figure 6, right side). These findings suggest that nonwovens with a high degree of fiber separation tend to exhibit greater repulsion

forces within the fabric, which negatively impacts their compressibility. The effect of chaotic filament orientation on compressibility was also demonstrated by Batch et al., who reported a notably reduced compressibility for such nonwoven structures [14]. In wet-laid nonwovens, generally, repulsion forces can be more effectively reduced compared to conventionally needled nonwovens, as the planar flow of water during manufacturing promotes an in-plane orientation of the filaments rather than alignment in the thickness direction. The fibers are still largely arranged chaotically within the plane, with numerous overlaps of individual filaments. When the nonwovens are compressed, the originally straight and stiff fibers become bent, a phenomenon that occurs significantly more often when fiber bundles are separated into single filaments and the number of fiber crossovers increases. Once the compression is released, the fibers tend to return to their original shape due to the elastic energy stored during bending. This phenomenon is commonly referred to as lofting and describes the 'spring-back effect' observed in more voluminous nonwoven materials. This suggests that, particularly in the case of single filament nonwovens, a certain degree of elastic repulsion force in the form of lofting is likely to occure during LSI process.

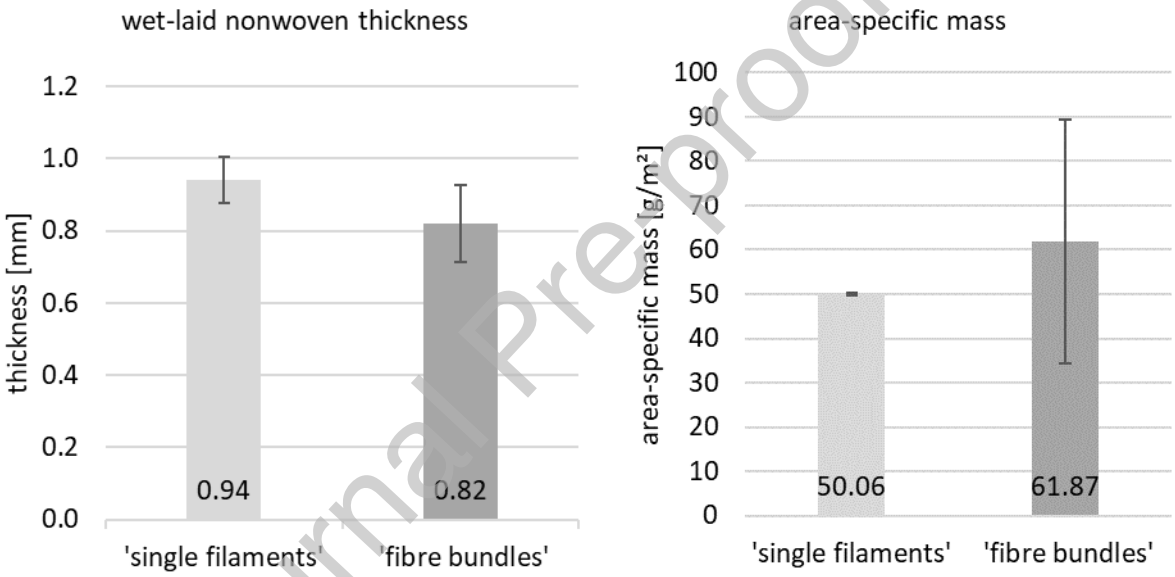

Figure 6 – Diagram of thickness (left hand side) and area related mass (right hand side) of wet-laid nonwoven

3.2 *In-situ* pyrolysis

The pyrolysis was carried out as described under 2.2. Due to the material transformation during pyrolysis, the image contrast changes while video recording. At the beginning fibers and matrix are clearly distinguishable, whereas with increasing temperature fibers and matrix become more similar in color and cracks become much more difficult to detect. In addition, the release of pyrolysis gases and the resulting cracks lead to movement of the sample, resulting in shifts in the original image section and temporary clouding.

Despite imperfect image quality during pyrolysis, the changes in the sample bodies could be sufficiently recorded. A list of all recognized effects is shown in Table 1, together with an assignment of the samples in which the respective effect occurred. Unfortunately, the video documentation of

sample 1 for the *fiber bundles* was not successful for technical reasons, which is why the assignment results for the sample are missing.

Table 1 – Occurring Effects during the *in-situ* pyrolysis of the two sample types

Tempera-ture [°C]	Effects	'single filaments'					'fiber bundles'				
		1	2	3	4	5	1	2	3	4	5
130 – 150	minor sample expansion	Y	Y	Y	Y	Y		Y	Y	Y	Y
190 – 320	Formation of horizontal cracks inside roving bundles (formation start 190 °C → max. widening 320 °C)				Y			Y	Y	Y	Y
300 – 345	Closure of horizontal cracks				Y			Y	Y	Y	y
300 – 340	Paused sample expansion	Y	Y	Y	Y	Y					
340 – 450	Further sample expansion	Y	Y	Y	Y	Y					
345 – 500	Paused sample expansion							Y	Y	Y	Y
450 – 610	Minor sample shrinkage	Y	Y	Y	Y	Y					
500 – 950	Sample shrinkage (only thickness direction) (start 500 °C, accelerated shrinkage at 600 °C, slowed down shrinkage at 750 °C until stop at 950°C)							Y	Y	Y	Y
610 – 710	Instantaneous formation of large crack network (manly horizontal orientation) with milder continuation until T = 710 °C	Y	Y	Y	Y	Y					
700 – 950	Formation of matrix cracks (vertical orientation) (start at 700 °C and continuation with moderate count of further cracks until 950°C)							Y	Y	Y	Y
710 – 950	Increased sample expansion in thickness direction (Lofting) but only minor crack formation	Y	Y	Y	Y	Y					

Two fundamental categories of effects were observed:

1. expansion/shrinkage of the material in Z-direction (specimen thickness)

2. formation of cracks between fibers and matrix, or in the matrix

Crack formation or closure cause expansion or shrinkage, even if shrinkage and expansion also take place without direct crack initiation. The two types of specimens differ fundamentally depending on the used fibers, as follows:

Single filaments: In the first phase, a slight expansion can be recognized, which continues up to approx. 300 °C. Then no further expansion is observed up to 340 °C Above 340 °C expansion continues up to approx. 450 °C with marks the beginning of the second phase. From then on, it switches to slight shrinkage, primarily in the Z direction (450 °C - 610 °C). At approximately 610 °C, a sudden and drastic formation of cracks distributed over the entire sample surface occurs, which continuously slowed down up to approx. 710 °C. However, the largest proportion of cracks occurs directly at the beginning. This event happens during the shift between phase 2 and 3. The formation of cracks also causes the sample thickness to expand abruptly. This is followed by only very little further growth of the crack network until the end of the experiment and happens in the third phase.

Fiber bundles: In the first phase (130 °C - 150 °C), slight expansion can be recognized, followed by first cracks forming at temperatures between 190 °C and 320 °C. The cracks are macroscopic and continuous and are located exclusively in fiber bundles along the fiber/matrix interface. In a relatively small subsequent temperature window (300 °C - 350 °C), most of the cracks close again. After that

the transition to phase 2 takes place while however, visually recognizable changes stagnate up to approx. 500 °C. From then until the end of the pyrolysis shrinkage of the matrix starts, which is primarily noticeable in the Z direction. Around the start of the third phase, larger cracks appear in the matrix from approx. 700 °C onwards. These and the previous cracks in the fiber bundles widen during the subsequent temperature increase (against the thickness shrinkage) and form the final crack network of the pyrolyzed samples.

Expansion / shrinkage analysis

The change in distance in in plane orientation (X and Y direction) and Z direction was determined by evaluating the taken videos via the software *Tracker* (Figure 7). The diagrams show the mean value of the respective sample types and the respective directions. For the *single filament* samples the tests could be evaluated up to approx. 610°C as with further increase in temperature the sample moved, preventing further measurements. For the *fiber bundles*, tracking was possible up to approx. 780°C. Beyond this temperature the change in contrast prevented further evaluation.

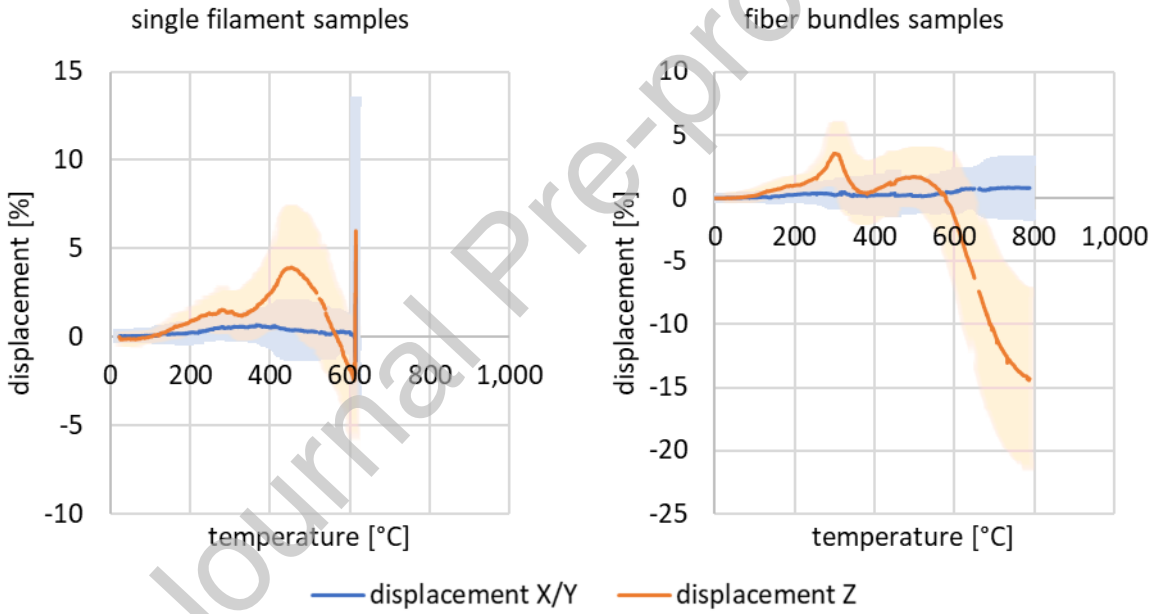

Figure 7 – Left: Distance change of the *single filament* samples in different spatial directions. Right: Distance change of the *fiber bundle* samples in different spatial directions.

For the *single filament* samples, two peaks are observed that indicate expansion in Z-direction (peak 1 at 290 °C, peak 2 at 450 °C) (Figure 7, left). They can be correlated with outgassing and with the onset of the pyrolysis. Between 450°C and 610°C the samples shrink considerably until abrupt crack network formation occurs and the samples therefore expand strongly. In in-plane direction no significant change could be detected and the displacement was always well below 1%.

Similar peaks were determined for the *fiber bundle* samples, but with certain shifts in the temperatures and the peak height (peak 1 at 310 °C, peak 2 at 500 °C) (Figure 7, right). Again, they indicate the outgassing above the consolidation temperature and the start of the carbonization regime. Due to larger crack openings in the fiber bundles the pyrolysis gases can be released easier

which results in a reduced swelling of the samples. Above 500 °C, the shrinkage continues until the end of the data acquisition to a reduced sample thickness of -14.3 % (780 °C). This observed shrinkage in thickness is consistent with the expected volume loss of the matrix during the carbonization regime and the subsequent dehydrogenation phase. For the in-plane orientation neither shrinkage nor expansion was observed (less than 1%).

After pyrolysis the *single filament* samples show an expansion of 45 % (mean value = 44.9 %, standard deviation = 8.9 %) which is attributed to lofting of the nonwoven preform. For the *fiber bundle* samples, the shrinkage is in the range of 14 % (mean value = -14.4 %, standard deviation = 4.1 %) which is relatively high compared to regular short fiber based CFRP for C/C-SiC, where the shrinkage is in the range of 1 to 5 % [15].

Crack formation

In total three crack formation events were observed: two for the *fiber bundle* samples and one for the *single filament* samples. All the events were observed at different temperatures resulting each in a different crack pattern.

Crack formation in *fiber bundle* type

First event: The first event occurs at a temperature between 150 °C and 345 °C (Figure 8). The cracks form in the area of the fiber bundles and do not extend into the matrix. The formation of these cracks begins at approx. 195 °C and coincides with the expansion observed in Z-direction. The expansion of the cracks peaks at approx. 300 °C. Further increase in temperature by only a few degrees (300 °C → 345 °C) leads to an almost complete closure of the cracks.

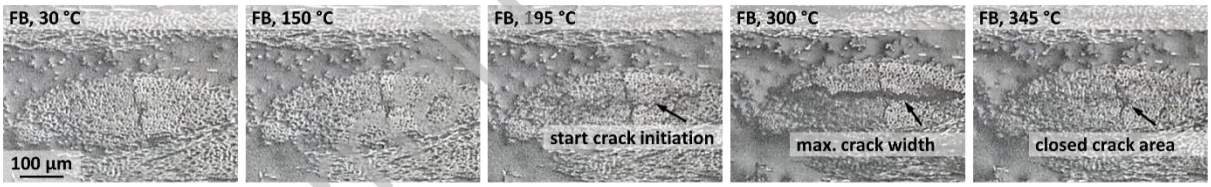

Figure 8 – Formation of macro cracks in fiber bundles between fiber/matrix interface during lower temperature range of the pyrolysis (30 °C – 345 °C)

Second event: Between approximately 600 °C and 900 °C, the matrix undergoes further conversion, and a second crack formation event occurs in the *fiber bundle* samples (Figure 9). In this temperature range, the matrix transforms from a polymer-like to a carbon-like structure (carbonization regime to hydrogenation). This process induces significant chemical changes, evident through a noticeable change in the matrix's color and contrast (Figure 9.3). Above 700 °C, cracks primarily form in matrix-rich regions and are characterized by a distinct vertical orientation. The matrix, unlike the fibers, experiences substantial shrinkage during this pyrolysis phase, which is responsible for generation of residual stresses. These stresses, in turn, lead to the formation of new cracks and the widening of pre-existing ones, such as those in the fiber bundles that formed during the first crack formation event.

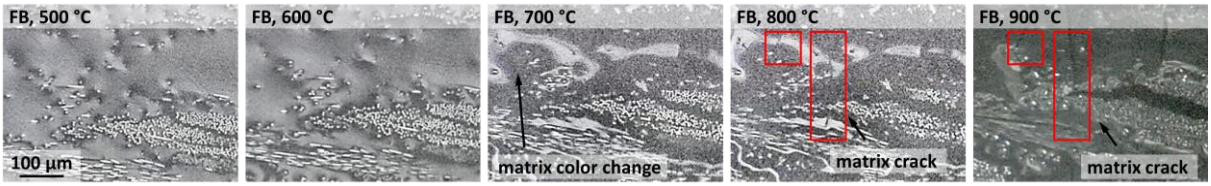

Figure 9 – matrix transformation and formation of vertical cracks in matrix on *fiber bundle* sample during dehydrogenation stage of pyrolysis (500 °C – 900 °C)

Crack formation in *single filament* type

In *single filament* samples, only a single crack formation event occurs, initiating abruptly at approximately 610 °C and reaching peak intensity near 640 °C. This event is characterized by the sudden development of a large number of predominantly horizontal cracks across the entire sample cross-section (Figure 10). The rapid formation of these cracks is accompanied by a pronounced increase in sample thickness. Beyond 640 °C, only minor changes in the crack pattern are observed up to 700 °C, indicating that the majority of the crack structure—relevant for the subsequent formation of the C/C-SiC composite—develops within this initial thermal interval. No further significant alterations in the crack morphology occur above this temperature range.

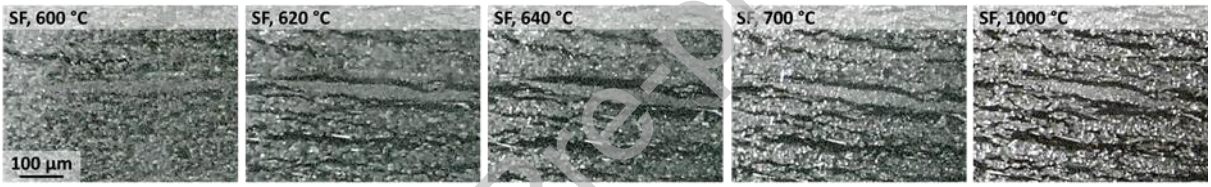

Figure 10 – instantaneous formation of massive crack network on *single filament* samples during dehydrogenation stage of the pyrolysis (600 °C – 1000 °C), with peak activity between 600 °C and 640 °C

3.3 Microstructure analysis

To analyze the microstructure, a ROI was identified per sample and analyzed before and after pyrolysis with a scanning electron microscope. The analyzed area before pyrolysis was 1000 µm in width by 1000 µm in length. The images after pyrolysis show the same ROI, but with the increase/decrease in thickness direction caused by the expansion/ shrinkage during pyrolysis.

For the *single filament* samples, in the CFRP state before pyrolysis the filaments are predominantly isolated (Figure 11). The fibers are primarily oriented in the X/ Y plane and not in the Z direction. The fiber/matrix bond seems to be strong and only a few pores can be seen. The identical ROIs after pyrolysis show a clear crack network with predominantly horizontal cracks, which branch out extensively and are connected to other cracks.

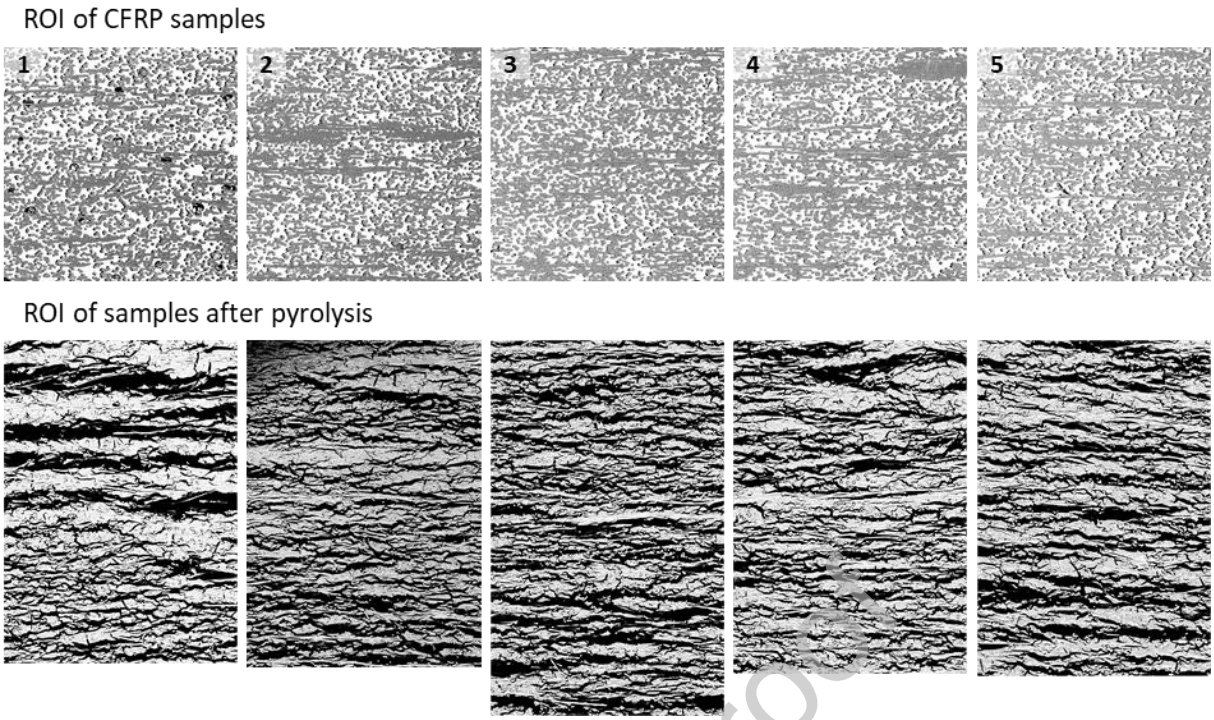

Figure 11 – ROI of the *single filament* samples before and after pyrolysis, with a pre-pyrolysis ROI equivalent to an area of 1000 µm × 1000 µm.

Detailed sections of the *single filament* samples are shown in Figure 12 (sample 4) to evaluate the type of cracks. The cracks after pyrolysis are a mixture of fiber/matrix detachments and cracks in the matrix. They are not separated from each other, but form a network.

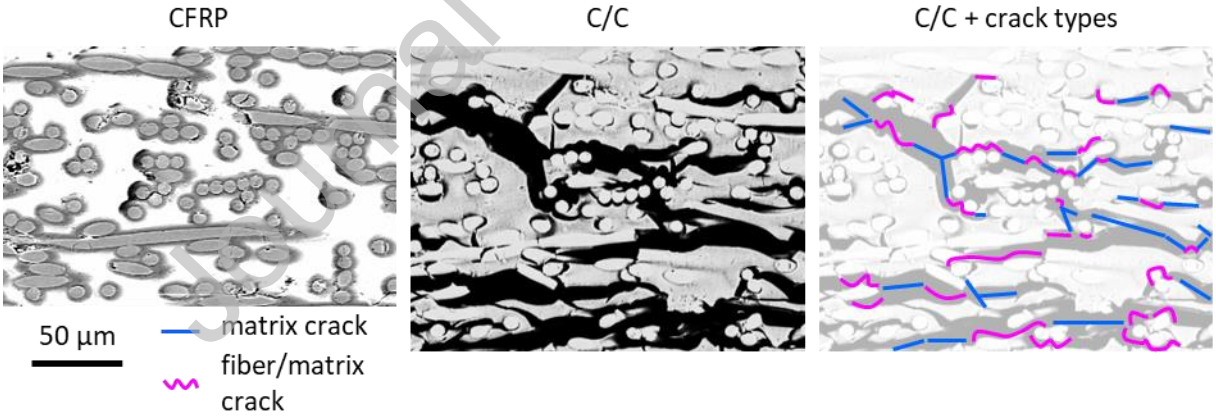

Figure 12 – Detailed view of the microstructure of *single filament* sample 4 before and after pyrolysis, with classification of the different cracks as either matrix cracks or fiber/matrix detachment.

For the *fiber bundle* samples, the microstructure in the CFRP state is displayed in Figure 13. Fiber bundles can be seen oriented in X/Y plane. The areas between the fiber bundles are filled with matrix and show isolated filaments, and in some cases less densely packed filament clusters (Figure 14, 4). After pyrolysis the ROI in the Z direction shrinked and additionally the crack network is formed. There are cracks in fiber bundles and cracks in the matrix. The crack network in the *fiber bundle* samples is

significantly less pronounced than in the *single filament* samples, which can be seen particularly clearly in sample five (Figure 13, 5).

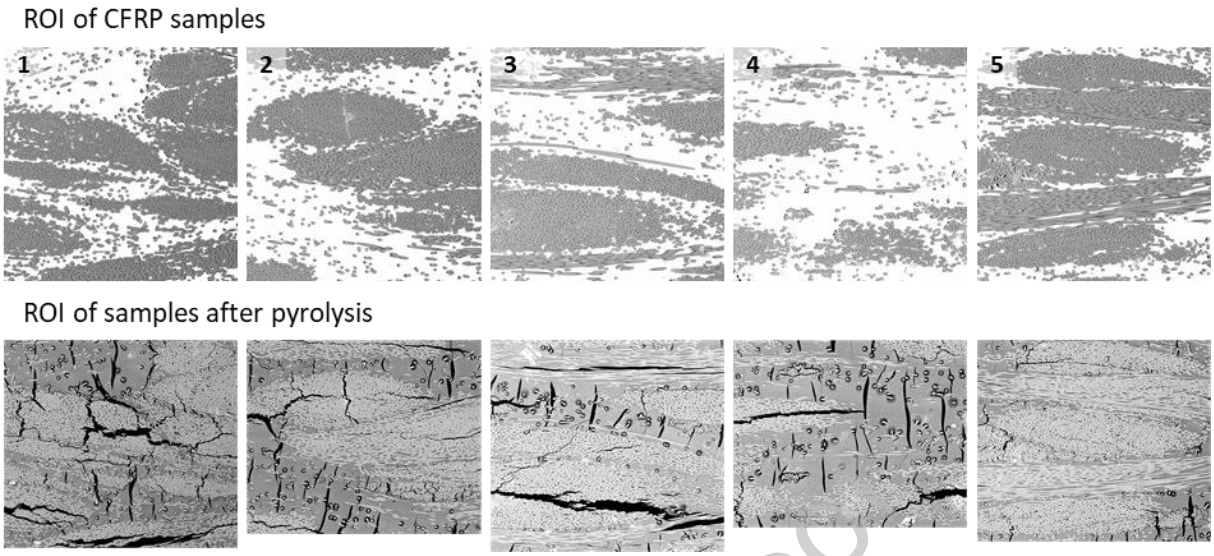

Figure 13 – ROI of the *fiber bundle* samples before and after pyrolysis, with a pre-pyrolysis ROI equivalent to an area of 1000 µm × 1000 µm.

Sample 3 (Figure 14) shows larger cracks within the matrix-rich areas resulting in cracks perpendicular to the fiber bundles and in cracks along the fiber matrix boundary.

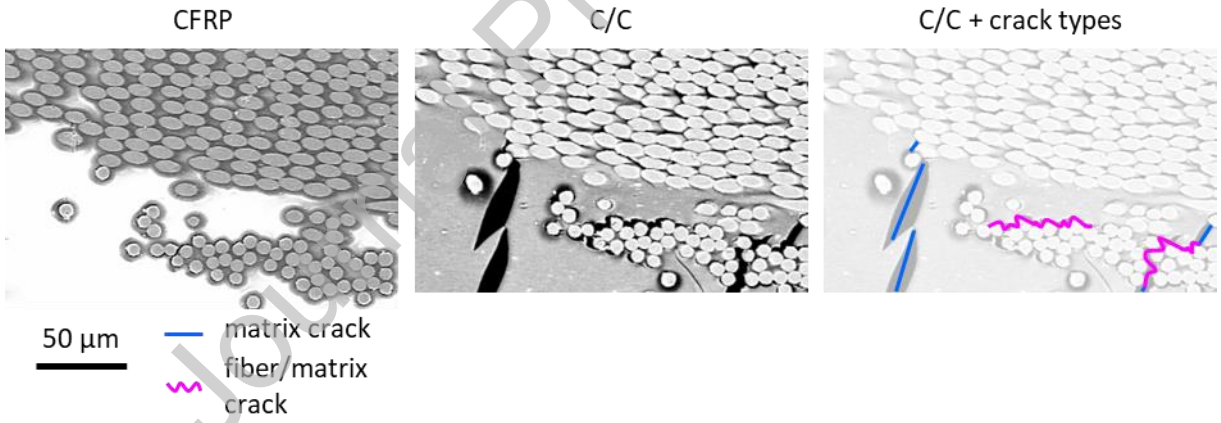

Figure 14 – Detailed view of the microstructure of *fiber bundle* sample 3 before and after pyrolysis, with classification of the different cracks as either matrix cracks or fiber/matrix detachment.

Fiber packing category analysis

To evaluate the influence of the packing density of the filaments on the crack network the images were analyzed using category analysis (Figure 15). The left diagram illustrates the relative distribution of each category across the two reinforcement types. For the *single filament* samples, 83% of all clusters fall within the medium fiber packing density range (28.5% to 68.8%), making this category clearly dominant. In contrast, for the *fiber bundle* samples the high category is most prominent (42%). However, the other categories also show substantial representation, each at 29%. This

distribution demonstrates that in the *fiber bundle* type, no category exhibits a strong dominance, while it does for the *single filament* type.

Following the categorization, the crack area within the region of interest (ROI) was analyzed for the pyrolyzed samples. Figure 15, right, shows the proportion of crack area within the cumulative categories for each sample type. For the *single filament* samples, the proportion of cracks across categories ranges between 34% and 46%. No distinct trend emerges that indicate a dominant occurrence of cracks in a specific category. For the *fiber bundle* samples, the proportion of cracks per category ranges between 7% and 10%, likewise showing no clear association between crack formation and a particular fiber packing density. Nevertheless, it is evident that the total crack area is significantly lower in *fiber bundle* samples compared to *single filament* samples.

These observations suggest that crack formation is a global phenomenon within both material types and cannot be solely attributed to localized variations in fiber packing density. However, as shown in Figure 13 (sample 5), local effects corelating to fiber packing density still occur. This sample exhibits a very high and highly concentrated fiber packing density, with minimal crack formation (individual result: 63% of clusters in the high category, 4% crack area within this category), indicating that local fiber architecture can still influence crack behavior to a certain extent.

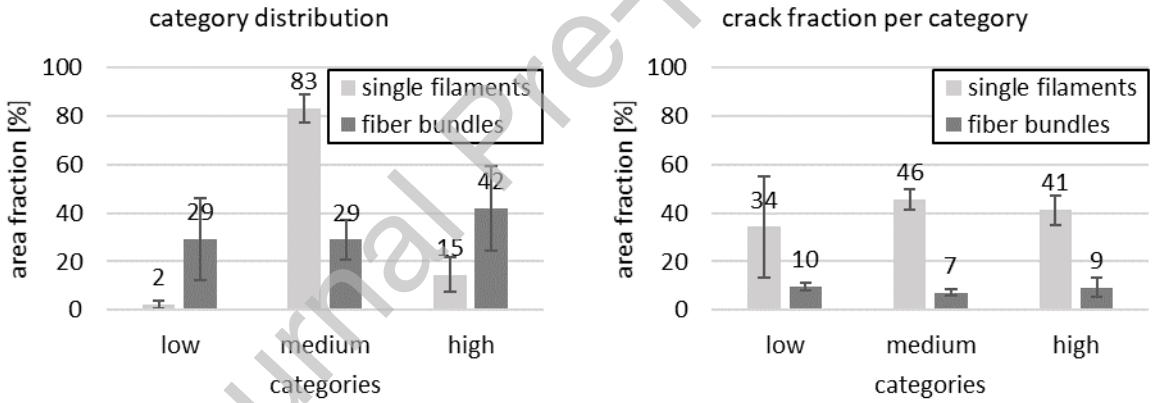

Figure 15 – Classification of fiber packing density according to the categories low, medium, and high, and assignment of the corresponding crack portion to the respective categories for *single filament* samples and *fiber bundles*.

Microstructure after siliconization

After the *in-situ* pyrolysis the samples were siliconized (Figure 16). The resulting composition corresponds to standard wet-laid nonwoven samples, as described in previous work (Figure 2) [1]. However, for the *single filament* samples, an increase in silicon and a decrease in silicon carbide were observed. While conventionally produced nonwoven C/C-SiC is pressed during processing in order to stabilize the shape throughout the process this was not possible for the *in-situ* pyrolyzed samples. Therefore, the lofting effect in these samples was pronounced leading to the resulting phase composition.

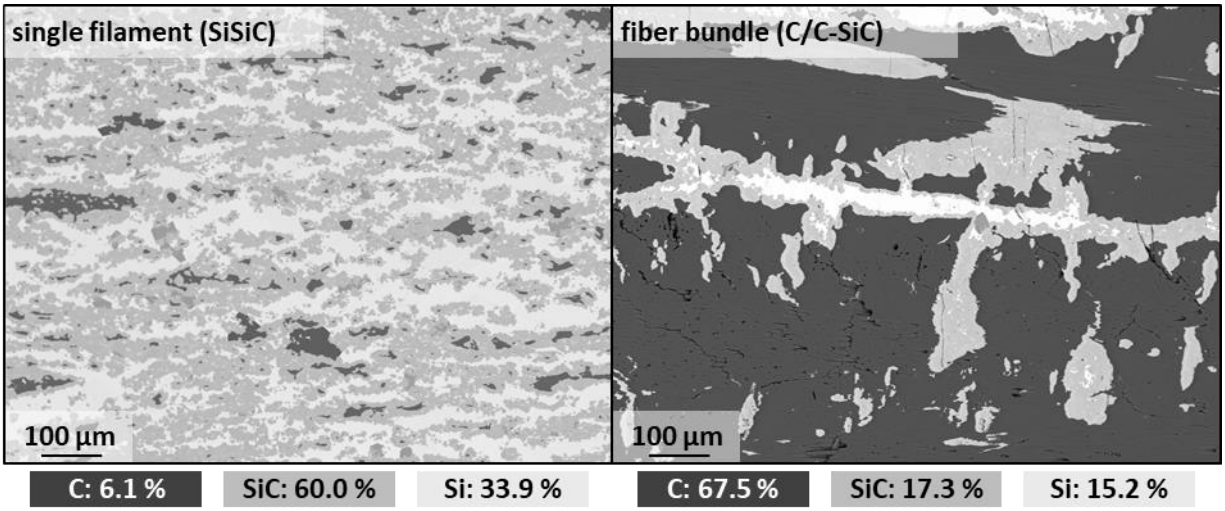

Figure 16 – Microstructure of siliconized samples from *in-situ* pyrolysis test, along with the corresponding phase composition.

3.4 Discussion

The analysis of the thermogravimetric results in combination with the observed phenomena during *in-situ* pyrolysis reveals that two principal types of effects occur throughout the process phases:

1. Shrinkage and expansion of the samples
2. Formation of cracks within the composite material

The occurrence of these events for both sample types is summarized in Figure 17 and highlights in particular how strongly crack formation is influenced by the preform. This applies not only to the morphology of the cracks but also to their respective temperature ranges.

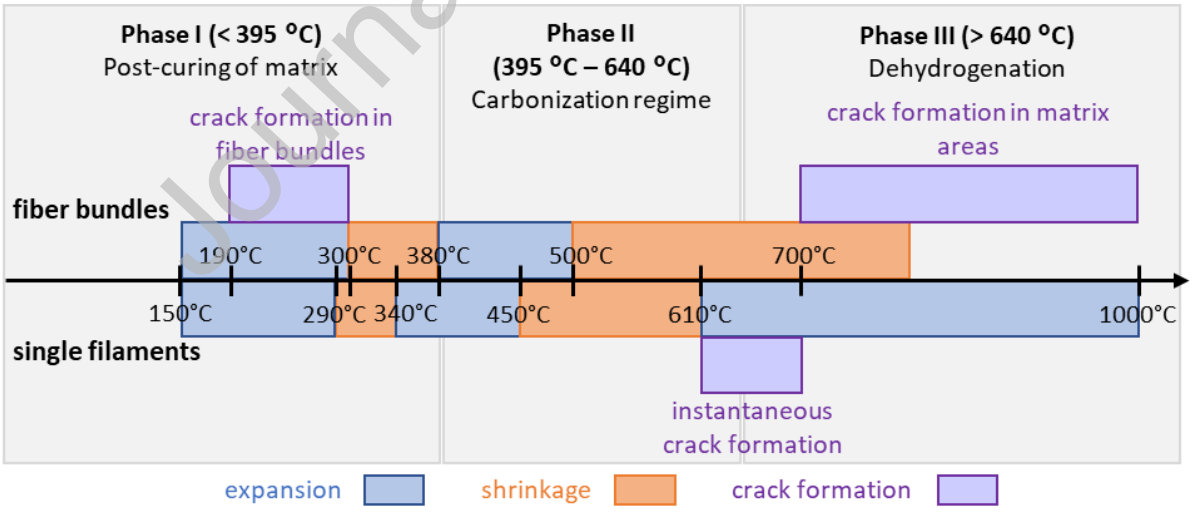

Figure 17 – Overview of the expansion, shrinkage and cracking effects that occur during pyrolysis

For the shrinkage and expansion different mechanisms are responsible. Expansion is primarily driven by outgassing and the cleavage of chemical reaction products, while shrinkage results from a volume reduction associated with the transformation of the polymer network into carbonaceous structures.

Two distinct expansion events are observed in both sample types, both primarily originating from reactions within the matrix resin. The first expansion occurs during the post-curing stage and is attributed to the evaporation of volatile phenol/cresol monomers and ongoing condensation reactions between functional groups in the resin, which lead to the release of water [9]. In addition, this expansion is supported by the initially slightly positive CTE of the phenolic matrix during the early phase of pyrolysis. The second expansionevent is observed at the end of the post-curing stage, marking the transition to the carbonization regime. It results from further chemical reactions that release typical pyrolysis gases such as water, methane, and carbon monoxide [9].

Shrinkage, on the other hand, is primarily caused by the loss of volatiles and the subsequent densification and reorganization of the carbon network. This transition from expansion to shrinkage occurs approximately midway through the main pyrolysis process—at around 500 °C for *fiber bundle* samples and at approximately 450 °C for *single filament* samples. Notably, no significant crack formation is observed at these transition temperatures, in contrast to fabric-reinforced C/C-SiC composites, where cracking typically begins at similar or lower temperatures [16].

For the second main effect – the crack formation- large differences between the two reinforcement types were observed.

Crack formation in *fiber bundle* type:

As previously described, the initial formation of cracks in *fiber bundle*-type preforms occurs between approximately 190 °C and 300 °C and is localized exclusively within the fiber bundles. At this stage, the cracks are characterized primarily by fiber/matrix debonding. According to Jain et al., significant negative thermal expansion occurs in pure phenolic matrix systems even at relatively low temperatures (150 °C to 290 °C) [13]. Although this thermal shrinkage contrasts with the overall macroscopic expansion behavior of the composite, it is crucial for understanding the origin of the first cracking event. The mismatch in thermal response—shrinkage of the matrix and expansion or stability of the fibers—generates internal mechanical stresses within the bundles. To relieve these stresses, cracks emerge and propagate in the direction of least resistance, which corresponds to the thickness direction of the composite.

The second cracking event begins during the dehydrogenation stage (Phase III). Shrinkage/expansion analysis reveals that the matrix undergoes its most pronounced contraction between 600 °C and 700 °C, with some shrinkage continuing beyond this range. At this point, the accumulated thermal stresses surpass critical limits, leading to matrix cracking. Compared to woven fiber-reinforced composites—where cracks are typically observed to initiate at lower temperatures (around 500 °C) [16]—the onset of cracking in nonwoven *fiber bundle* systems is delayed. In woven structures, the highly oriented filaments strongly restrict matrix shrinkage, leading to early transverse cracking due to the mismatch in thermal expansion between the matrix and the dimensionally stable fibers [12]. In contrast, the wet-laid nonwoven architecture lacks such preferential orientation and typically exhibits a lower fiber volume fraction (ca. 30% vs. 60% in woven textiles). This results in less constrained matrix shrinkage and a more gradual buildup of thermal stresses. Observations by Trick et al. confirm that in these systems, matrix shrinkage initiates around 500 °C [9]. Although matrix shrinkage initiates around this temperature, the accumulation of thermal stress becomes critical only between 650 °C and 700 °C, leading to crack formation. This corresponds to the temperature range in which the critical shrinkage rate is reached and the onset of matrix cracking is observed. These matrix

cracks then propagate and merge with existing damage in the fiber bundles, leading to the final crack pattern by so-called interconnection mechanism. These findings align with the conclusions made by Fischedick et al., indicating that the primary mechanism driving crack formation is not pore pressure from pyrolysis gases, but rather the mechanical stresses between the shrinking matrix and the dimensionally stable fibers.

Crack formation in *single filament* type:

In the *single filament* samples, only one major crack formation event is observed, initiating at approximately 610 °C. This results in an unusual crack morphology for CMC materials, characterized by a highly branched crack network and a total pore volume of up to 40%. The underlying mechanisms differs substantially from those in *fiber bundle*-type materials.

During the temperature range in which the first crack formation occurs in *fiber bundle* samples, no damage is observed in the *single filament* samples. This can be attributed to the absence of fiber bundles. Instead, the fibers are distributed isotropic within the plane, preventing localized stress accumulation due to thermal expansion mismatch between fibers and matrix. As pyrolysis progresses, a critical transition occurs at around 610 °C. Ko et al. and Wielage et al. have shown that the morphological change near 600 °C in phenolic resin-based composites - transforming from polymer-like chains (< 600 °C) to a carbon network (> 600 °C) leads to a temporarily loss of mechanical integrity [17, 18]. The original crosslinked structure is degraded before the new carbon network is fully established. This weakened matrix phase makes the composite particularly vulnerable to mechanical stresses. Such stresses are already present in the material due to the compression process during CFRP fabrication and are released as the material tends to return to a less compressed state (lofting).

In combination with the structurally weakened matrix at around 600 °C, this release triggers the formation of the highly branched crack network. Microstructural analysis supports this interpretation, showing widespread and simultaneous matrix cracking and fiber/matrix debonding, suggesting failure driven by accumulated internal force.

While the described crack formation mechanisms illustrate how strongly the evolving microstructure is influenced by the type of the preform, the categorization of samples by local filament density in correlation with crack formation showed little to no impact on the resulting crack patterns (Figure 15). Although the crack morphology clearly depends on the type of preform (*single filaments* or *fiber bundles*), this effect does not stem from filament packing density alone, but rather from the extent to which filament orientation facilitates dense packing. This is supported by the observation that no correlation was found between local fiber packing density and crack formation, but rather a global correlation between crack density and preform type.

4 Conclusion

This work explains the effects that occur during pyrolysis in wet-laid nonwoven-based C/C-SiC ceramics depending on fiber distribution by use of *single filament* or *fiber bundles* as reinforcement. The properties of the resulting fiber preform induces different crack patterns compared to those found in fabric reinforced ceramics and changes the microstructure evolving during the pyrolysis. For ceramics with *fiber bundle*-based reinforcement, cracks only occur during post-curing (195 °C to 300 °C) and when the matrix has significantly shrunk at temperatures above 700°C. For *single filament*-

based ceramics, the key effect is the release of forces arising from the poor compressibility of nonwovens with heavily separated filaments and chaotic layout. When these forces are released during pyrolysis a 'lofting' effect occurs which results in a high thickness expansion of the material. The highly branched crack network leads to extremely high accessibility of the C/C structure for silicon infiltration and ultimately to a largely monolithic SiSiC-dominated ceramic material. The influence of the fiber preform is significant for the microstructure and ultimately plays a crucial role in the effects that occur during pyrolysis. These effects need to be considered when aiming for wet-laid nonwoven-based ceramics with specific properties such as fracture toughness in the *fiber bundle* type or high wear resistance in the *single filament* type.

5 Credit authorship contribution statement

F.K. designed, conducted, and analyzed experiments and wrote the manuscript. T.B., A.M., N.H. and L.B. designed and conducted experiments and edited the manuscript. D.K. and M.F. designed and analyzed experiments and edited the manuscript.

6 Data availability

Data will be made available on request.

7 Acknowledgment

This research is funded by the German Aerospace Center. The authors would like to sincerely thank, Felix Vogel and Marco Alexander Smolej, at the DLR-Institute of Structures and Design for their technical support.

8 References

1. Kessel, F., et al., *Wet-laid nonwoven based ceramic matrix composites: An innovative and highly adaptable short fiber reinforcement for ceramic hybrid and gradient materials.* Journal of the European Ceramic Society, 2021. **41**(7): p. 4048-4057.
2. Shideler, J.L., G.L. Webb, and C.M. Pittman, *Verification tests of durable thermal protection system concepts.* Journal of Spacecraft and Rockets, 1985. **22**(6): p. 598-604.
3. Tenney, D.R., W.B. Lisagor, and S.C. Dixon, *Materials and structures for hypersonic vehicles.* Journal of Aircraft, 1989. **26**(11): p. 953-970.
4. Krenkel, W.K., R. , *The LSI Process - A Cost Effective Processing Technique for Ceramic Matrix Composites.* Int. Conf. on Advanced Materials, Beijing / China, 12-15 Aug. 96, 1996: p. 5.
5. Suzuki, T., T. Miyajima, and M. Sakai, *The role of the fiber/matrix interface in the first matrix cracking of fiber-reinforced brittle-matrix composites.* Composites Science and Technology, 1994. **51**(2): p. 283-289.
6. Krenkel, W. and F. Reichert, *5.1 Design Objectives and Design Philosophies, Interphases and Interfaces in Fiber-Reinforced CMCs*, in *Comprehensive Composite Materials II*, P.W.R. Beaumont and C.H. Zweben, Editors. 2018, Elsevier: Oxford. p. 1-18.
7. Kessel, F., et al., *Three-dimensional preforming via wet-laid nonwoven technology for ceramic matrix composites.* Journal of the European Ceramic Society, 2023. **43**(12): p. 5148-5158.
8. Jenkins, G.M. and K. Kawamura, *Polymeric Carbons: Carbon Fibre, Glass and Char*. 1976: Cambridge University Press.
9. Trick, K.A. and T.E. Saliba, *Mechanisms of the pyrolysis of phenolic resin in a carbon/phenolic composite.* Carbon, 1995. **33**(11): p. 1509-1515.
10. Torres-Herrador, F., et al., *Decomposition of carbon/phenolic composites for aerospace heatshields: Detailed speciation of phenolic resin pyrolysis products.* Aerospace Science and Technology, 2021. **119**: p. 107079.
11. Schulte-Fischedick, J., et al., *Crack Microstructures During the Carbonizing of Carbon Fiber Reinforced Plastics to Carbon/Carbon Composites*. 1999. 60.
12. Schulte-Fischedick, J., *Formation of crack pattern during pyrolysis of carbon fiber reinforced composites for production of C/C materials.* DLR Deutsches Zentrum fur Luft- und Raumfahrt e.V. - Forschungsberichte, 2005: p. 1-192.
13. Jain, N., et al., *Characterization and modeling of transverse micro-cracking during pyrolysis process of carbon fiber reinforced plastics.* International Journal of Applied Ceramic Technology, 2019. **16**(5): p. 1734-1743.
14. Batch, G., S. Cumiskey, and C. Macosko, *Compaction of fiber reinforcements.* Polymer Composites, 2002. **23**: p. 307-318.
15. Heidenreich, B., R. Renz, and D.W. Krenkel, *Short Fibre Reinforced CMC Materials for High Performance Brakes*, in *High Temperature Ceramic Matrix Composites*, D.W. Krenkel, P.D.R. Naslain, and P.D.H. Schneider, Editors. 2001. p. 809-815.
16. Schulte-Fischedick, J., et al., *The crack development on the micro- and mesoscopic scale during the pyrolysis of carbon fibre reinforced plastics to carbon/carbon composites.* Composites Part A: Applied Science and Manufacturing, 2007. **38**(10): p. 2171-2181.
17. Wielage, B., et al., *Thermo-Mechanical Monitoring of Composite Materials during the Pyrolysis of C/C Composites.* Key Engineering Materials, 2010. **425**: p. 95-105.
18. Ko, T.-H., W.-S. Kuo, and Y.-H. Chang, *Microstructural changes of phenolic resin during pyrolysis.* Journal of Applied Polymer Science, 2001. **81**(5): p. 1084-1089.

Graphical Abstract

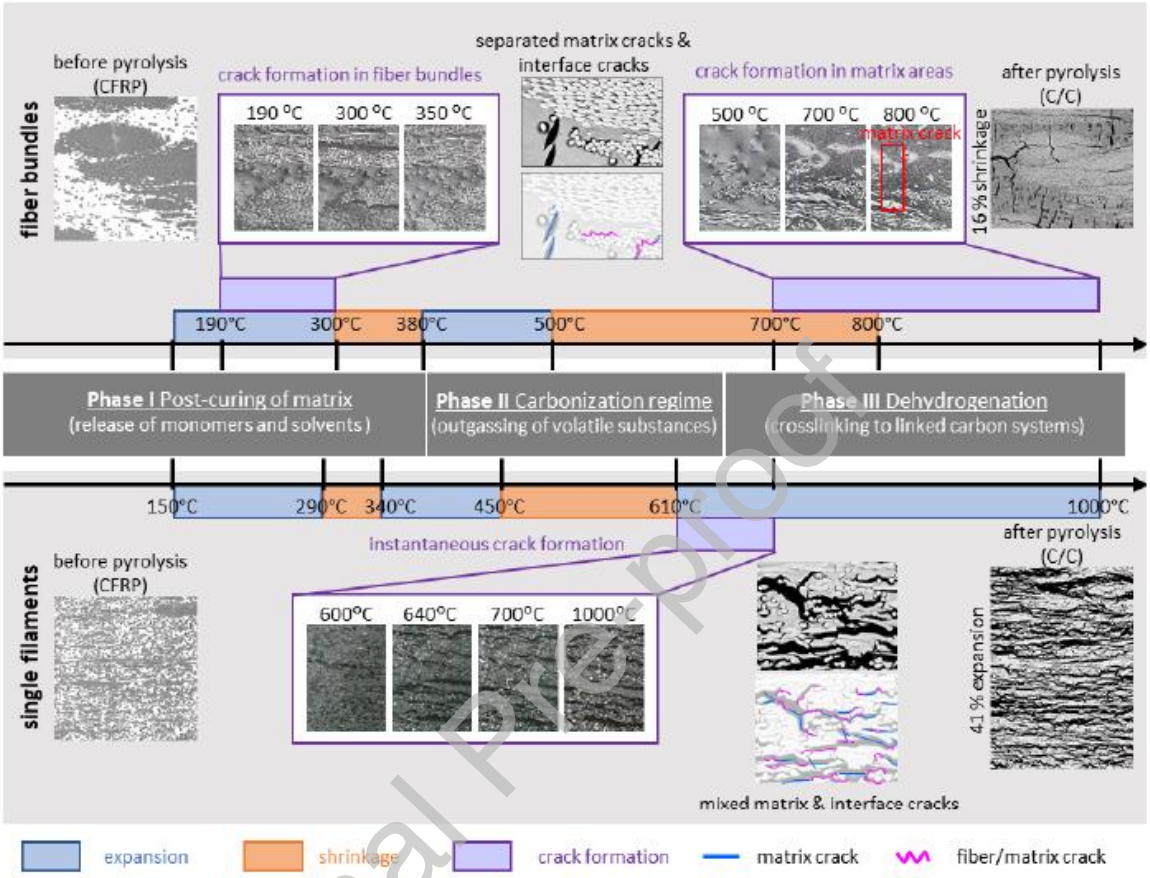

Declaration of interests

☒The authors declare that they have no known competing financial interests or personal relationships that could have appeared to influence the work reported in this paper.

☐The authors declare the following financial interests/personal relationships which may be considered as potential competing interests:

R